CHAPTER 177

Beach Response in Front of Wave-Reflecting Structures

Roy C. Seaman[1] and Tom O' Donoghue[2]

Abstract

The results of an experimental study of beach response in front of wave-reflecting structures are presented. The particular beach response problem is the so-called "N-type" response where sand is eroded in the area between the node and antinode and is transported towards the node. The characteristics of the equilibrium beach profile are presented and an equation describing the profile is proposed. The beach response is fundamentally dependent on the interaction between the flow and the ripples superimposed on the larger bedforms. Particle image velocimetry (PIV) has been used to look closely at the ripples and the flow. It is found that the sand transport towards the node results from larger vortex growth on the antinodal side of ripples than on the nodal side caused by the asymmetry in the main flow velocity time history which itself is a result of the superposition of the non-linear incident and reflected waves.

Introduction

Under a standing wave two main types of sediment transport can occur: transport of sand in suspension from under nodes towards antinodes or transport of sand as bed-load from between node and antinode towards the node. The former is often referred to as "L-type" movement and the latter as "N-type" movement. Previous notable research in this area (de Best *et al* (1971), Irie and Nadaoka (1984) and Xie (1985)) has shown that a "movability parameter", defined as the ratio of shear velocity to sediment fall velocity, can be used to determine which of the two types of transport is likely to occur for a given set of conditions. For relatively low values of the movability parameter, beach material transport is N-

---

[1]) Research Student, University of Aberdeen, Department of Engineering, King's College, Aberdeen AB24 3UE, Scotland, U.K.

[2]) Lecturer, University of Aberdeen, Department of Engineering, King's College, Aberdeen AB24 3UE, Scotland, U.K.

type and for relatively high values of the movability parameter, the transport is L-type.

N-type movement is demonstrated very easily in the laboratory by sprinkling some sand onto a fixed flat bed: under a standing wave the sand, provided the movability parameter is sufficiently low, oscillates on the bed and gradually advances towards the node. The reason why this occurs is because the direction of mass transport at the bottom of the wave boundary layer under a standing wave is towards the node as described originally by Longuet-Higgins (1953) and, in the context of the development of offshore sand bedforms, by Carter, Liu and Mei (1973). However, for a fully-mobile bed under a standing wave, ripples form very quickly and subsequently play a crucial role in the sand transport process.

The present paper presents the results of an experimental investigation of N-type beach response. Two main aspects of the problem are addressed: first, the characteristics of the "equilibrium" beach profile and, second, the fundamental dependence of the sand transport on the interaction between the flow and the ripples superimposed on the larger bedforms.

Experimental Set-up

All experiments were conducted in a 20m long, 0.45m wide random wave flume with a water depth at the paddle of 0.7m (Figure 1(a)). A horizontal tray, approximately 3m long and supported in the wave tank by a frame fixed to the tank, held a 200mm deep sand bed, the top 100mm or so consisting of a well-sorted sand with D_{50}=0.32mm. A vertical, impermeable wall was located at the shoreward end of the sand bed. The water depth in front of the wall was 150mm. Waves approached the sand bed from the deeper 0.7m depth at the paddle via a sloping false floor with a 1:20 slope over most of its length and constructed from perspex panels supported on an aluminium frame.

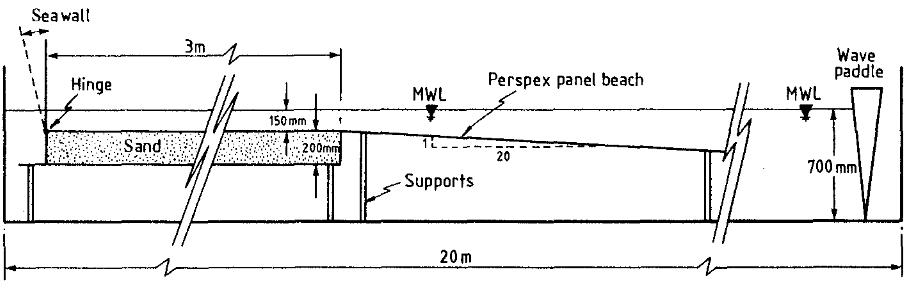

Figure 1(a): Experimental Set-up

Seventeen experiments corresponding to a wave frequency range of 0.7-1.1Hz and incident wave height range of 30-60mm were conducted in which the bed development from flat bed to equilibrium profile was observed. Once the equilibrium condition was reached for a given wave condition, the water level in the tank was lowered and the beach measured using a laser displacement sensor. The sensor has a spot diameter of 1mm and a resolution of 50μm and was mounted on a computer-controlled x-y table. For each experiment a total of 31 profiles were measured at 10mm intervals across the wave tank over a 300mm wide central section and at a resolution of 2mm in the longitudinal direction stretching from the wall to the first offshore antinode.

In order to study the underlying processes of the beach response, the detailed flow behaviour for a single wave condition (f = 0.9Hz and H = 50mm) was examined using particle image velocimetry (PIV). At selected stages in the development of the beach profile the bed was made rigid by sprinkling a thin layer of cement over the bed and allowing it to harden. PIV was then used to measure the instantaneous 2-d velocity field over and around individual ripples at selected phases of the wave cycle.

The PIV system used is based on a cross-correlation camera with two 756x458 CCD arrays. The camera is part of a completely integrated imaging system which includes the camera, PCI frame-grabber and camera-control card and Windows-based image acquisition and processing software. The camera views a part of the seeded, illuminated flow-field. Illumination was achieved using an 18W argon-ion laser beam carried by fibre-optic cable to a rotating mirror positioned above the wave tank which directed the beam via a lens to a thin sheet of glass held semi-immersed in the water (Figure 1(b)). The plane of the glass sheet was perpendicular to the mean water level and parallel to the sides of the wave tank. The purpose of the glass sheet was to avoid problems associated with bringing the laser beam through a fluctuating air-water interface. The light sheet was approximately 300mm long but only a fraction of this was viewed by the camera when measuring flow over the ripples.

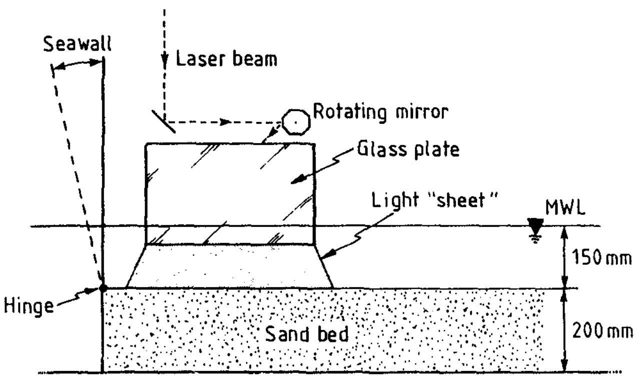

Figure 1(b): Illumination for PIV

Overview of Beach Response

Figure 2 illustrates the typical development of the beach with time from the initial flat bed condition to the final, equilibrium profile. At the beginning of an experiment sand on the flat, horizontal bed began to oscillate back and forth. Oscillations were most vigorous underneath the node where velocity amplitudes were highest resulting in the rapid development of ripples here. Ripple formation then propagated towards the antinodes on either side until a point was reached beyond which the near-bed velocities were too low to initiate movement of the sand. These points are referred to as the limits of movement in the present paper. The ripple wavelength and height decreased with distance from the node, a result which is consistent with the reduction in the radius of water particle orbits with distance from the node. The characteristics of the ripples remained largely unchanged throughout the experiment as the underlying larger bedform developed. Beach development progressed as sand continued to move towards the node from the areas close to the limits of movement resulting in areas of scour adjacent to the limits of movement and a zone of accretion around the node. The scour holes deepened with time and velocities within the scoured areas decreased until no further sand transport could occur. At this stage sand movement towards the node ceased. Sand close to the node continued to oscillate back and forth under the high velocity amplitudes present there, but no further net transport was produced and the bed was said to have reached "equilibrium".

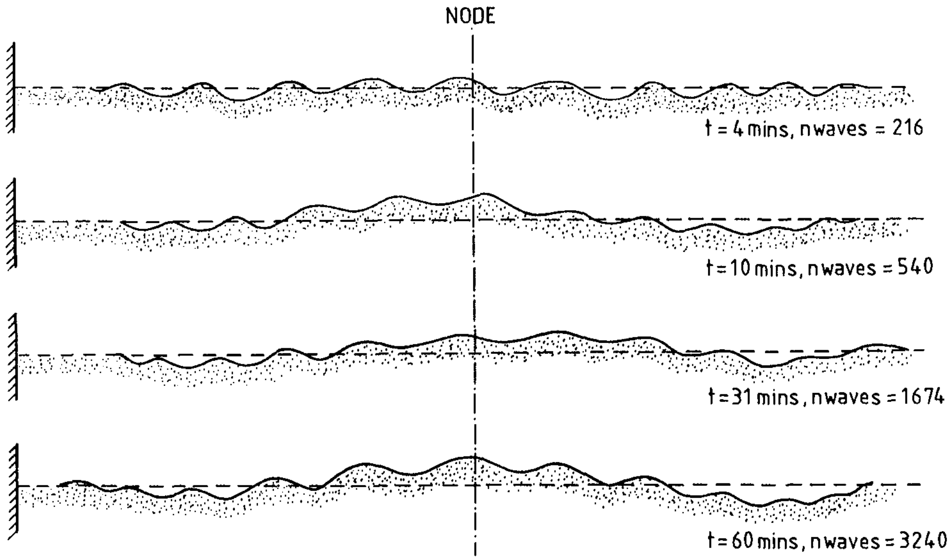

Figure 2 Sample beach profiles through time for f =0.9Hz and H=0.05m

The Equilibrium Profile

The underlying larger bedform of the equilibrium profile is of significant engineering interest. The following equation is proposed to describe its major features:

for $x_l \le x \le (\frac{\lambda}{2} - x_l)$
$$\eta_b = \frac{a}{3}\sin\left\{\frac{2\pi}{3\lambda_b}(x - x_l)\right\} - a\sin\left\{\frac{2\pi}{\lambda_b}(x - x_l)\right\} \quad \text{...[1]}$$

where x is distance from the wall, x_l is the distance from the wall to the first limit of movement (equal to the distance from the second limit of movement to the offshore antinode), λ is the wave wavelength, η_b is the bed elevation above the initial flat bed level, a is a measure of the amplitude of the profile and λ_b is the bed profile wavelength where

$$\lambda_b = \frac{4}{3}\left(\frac{\lambda}{4} - x_l\right) \quad \text{...[2]}$$

For a given incident wave wavelength the function is fully defined if the positions of the limit of movement x_l and the amplitude factor a are known. The integral of the function over a half wavelength (antinode to antinode) is zero. The highest point on the profile is

$$\eta_{b_{max}} = \frac{4}{3}a \quad \text{...[3]}$$

The maximum scour depth is $\eta_{b_{min}} = -\frac{5}{6}a$ ...[4]

For a given measured profile the limits of sand movement can be determined by calculating the local bed gradient as one advances from the antinode (where the bed gradient is zero) to a point where the gradient suddenly changes. The a value is then determined from a least squares regression of equation [1] onto the measured data. Two examples of measured profiles and their corresponding fitted functions are presented in Figure 3. Generally the function provides a good fit to the overall bed profile shape: it picks out the positions of maximum accretion and maximum scour satisfactorily and the method used to establish the limits of movement is seen to be successful. However, the function does tend to slightly under-predict the maximum scour and the gradient of the slopes leading up to the peak.

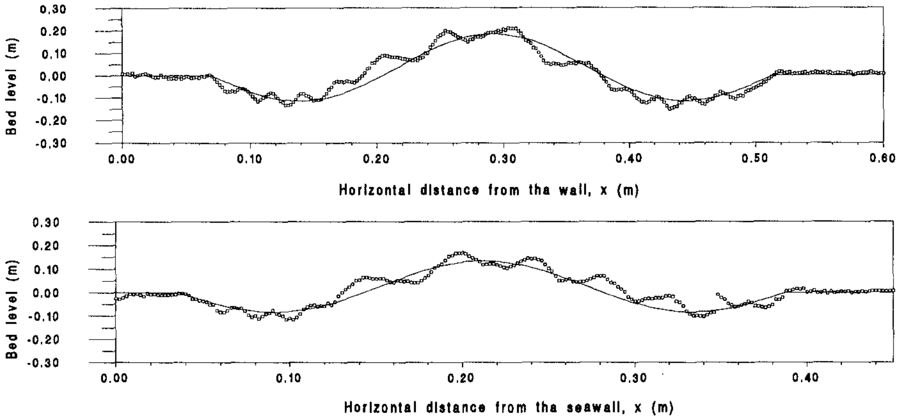

Figure 3: Measured profiles and corresponding best-fit of equation [1]. Top: f=0.9Hz, H=30mm; Bottom: f=1.1Hz, H=40mm

The values of x_l were determined for each of the 31 longitudinal profiles of each experiment. Of course two limits are obtained for each profile: the first limit is the shoreward limit denoted x_{l1} (i.e. the limit closest to the wall); the second is the seaward limit and is denoted x_{l2}. Figure 4 shows the results obtained for the limits of movement for three different wave period conditions. The results show the expected shift seaward of the limits of movement as the wave period increases, reflecting the seaward shift of the node of the standing wave. The results also show that the limits of movement are generally reasonably consistent across the width of the wave tank, significant scatter being observed only in the seaward limit of the longest period waves.

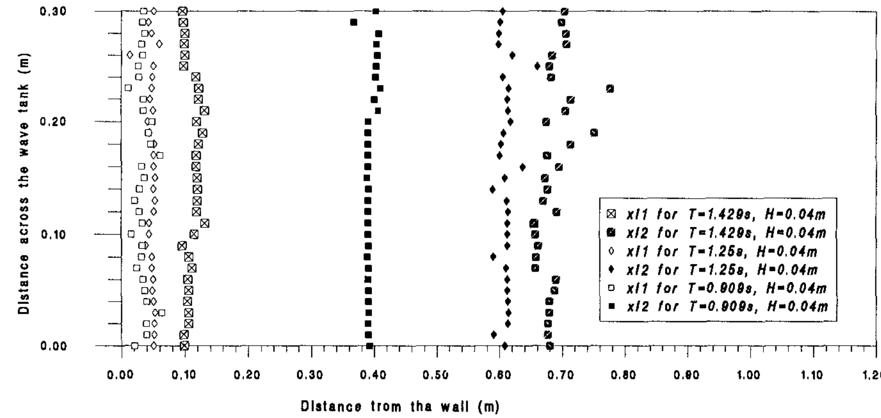

Figure 4. Measured limits of movement for 3 experiments.

A comparison of the measured limits of movement with the limits predicted using an incipient motion criterion is presented in Figure 5. The incipient motion criterion used is that proposed by Losada and Desire (1985) given by

$$\frac{A}{D_{50}} = \alpha' \left(\frac{\mathrm{Re}^{\frac{2}{3}}}{D_*} \right)^{6/5} \quad with \quad D_* = D_{50} \left(\frac{\gamma g}{\upsilon^2} \right)^{1/3} \quad and \quad \mathrm{Re} = \frac{u_{max} A}{\upsilon} \qquad \ldots[5]$$

where A is the amplitude of water particle excursion at the bed, D_{50} is the sediment size, γ is sediment specific gravity, υ is kinematic viscosity and u_{max} is the amplitude of horizontal water particle velocity at the bed. A limited study on the point of incipient motion of the sand used in this study was undertaken prior to the main body of experiments. For a number of wave periods, the wave height was increased in increments of 10mm until a value was reached at which movement of the sand could be clearly seen. The positions of the two points, one either side of the node, marking the separation of the area of bed where sand moves and the area where no sand movement occurs were measured and from this a threshold velocity calculated. The results obtained agreed very well with Losada and Desire's presentation of Goddet's data with α' equal to 1.34.

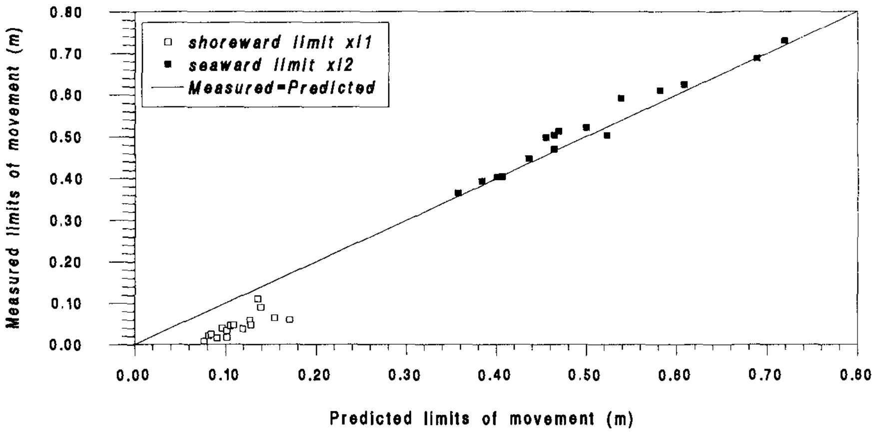

Figure 5 Comparison of predicted and measured limits of movement.

In Figure 5 the measured limits of movement are the average values of the 31 profiles. Figure 5 shows that the seaward limits of movement of the equilibrium profiles are well predicted using the incipient motion criterion. However, there is poor agreement between the measured and predicted shoreward limits. It is not known at this stage why this should be the case: the measured results suggest that the threshold velocity for sand movement near the wall is less than the threshold velocity away from the wall; of course the predicted threshold velocity is the same at the seaward and shoreward predicted limits of movement.

Although care was taken during the experiments to ensure that the wall was perfectly perpendicular to the incident waves, the response of the beach was never perfectly 2-dimensional, i.e. the beach profile varied across the width of the tank. Some evidence of this was seen in Figure 4 in respect of the limits of movement. Figure 6 shows the variation in *a* across the width of the tank for three different wave periods; *a* has been non-dimensionalised with respect to the mean value of the 31 *a* values of each test. The results show that *a* can deviate from the mean *a* value by as much as 20% of the mean value. This is an important result in that it illustrates the extent to which the developed beach is not perfectly 2-dimensional and reveals the dangers of obtaining results from a single longitudinal profile.

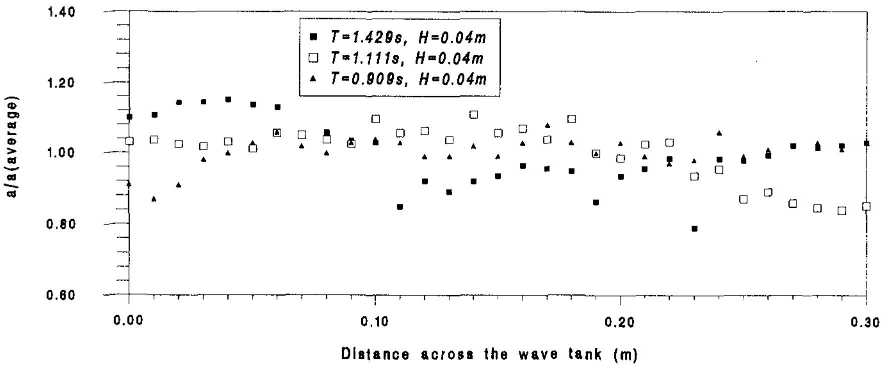

Figure 6 Variation in *a* across the wave tank for three example conditions.

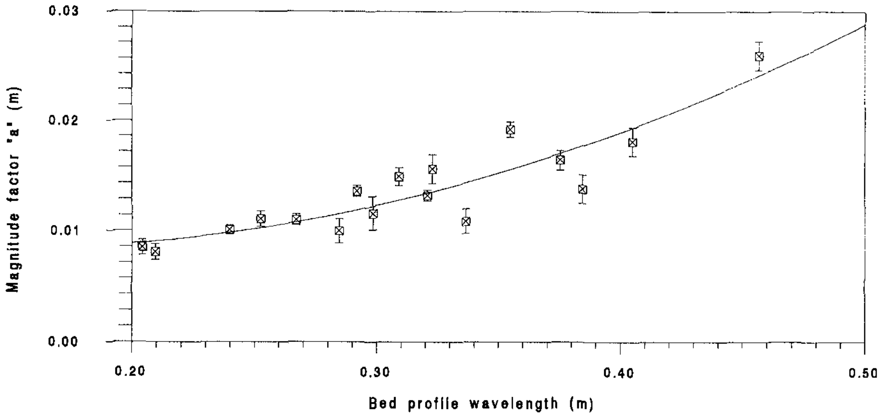

Figure 7: Relationship between the amplitude and wavelength of the equilibrium bed profile.

The average a and its standard deviation was calculated from the 31 profiles of each experiment. The average bed profile wavelength λ_b was calculated from the measured limits of movement of the 31 profiles. Figure 7 shows the plot of average a against average λ_b, the error bars on a corresponding to $\pm$ the standard deviation of a. Although there is some scatter, there is a reasonably good correlation between a and λ_b, particularly at lower values of λ_b. The results show that, for the conditions of the present study, the value of a is between 1/20th and 1/30th of the bed profile wavelength λ_b.

Mechanism of Sand Transport Towards the Node

During the very early stages of the beach development the primary mechanism causing sand transport towards the node is mass transport at the bottom of the wave boundary layer as described by Carter, Liu and Mei (1973). However, as the ripples grow, first at the node and later further out, they become large enough to shed vortices. Observations indicated that these vortices then become the dominant mechanism in further sand transport. In order to study the behaviour of the vortices, a single experimental condition was selected (f = 0.9Hz, incident H = 50mm) and flow around the ripples was studied using PIV.

Before looking at some of the PIV results it is first necessary to look at the characteristics of the main flow, i.e. the flow at a position away from the bed. LDA measurements of velocity were made at a height of 25mm above the initial flat bed at 8 positions in front of the reflecting wall. Figure 8 presents the results for the horizontal component of velocity along with a prediction of the horizontal velocity based on the superposition of two Stokes second order waves. There is good agreement between the measured and predicted velocity time series. The maximum velocity towards the wall (positive velocity) and away from the wall (negative velocity) are approximately equal to each other at each of the 8 positions. However, the velocity function is generally asymmetrical, meaning that accelerations are not of the same magnitude in the two directions. For example, at position 1 maximum acceleration away from the wall is much greater than the maximum acceleration towards the wall, or, in other words, acceleration is greater towards the node; at the corresponding position on the other side of the node, position 7, maximum acceleration towards the wall is much greater than that away from the wall, or, again, maximum acceleration is greater towards the node. So, maximum acceleration is always greater towards the node than away from the node and, because the degree of asymmetry decreases as the node is approached, the difference between maximum acceleration towards and away from the node decreases as the node is approached.

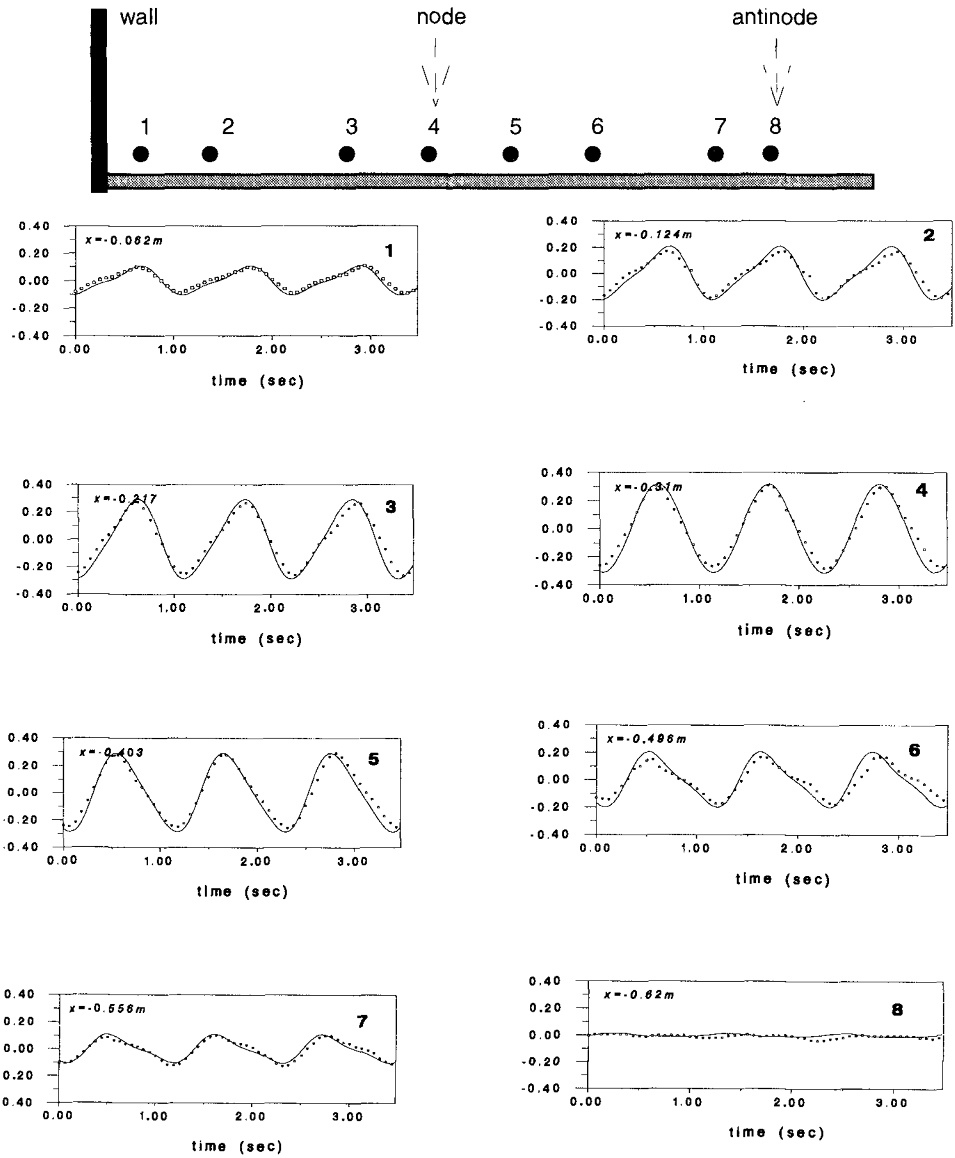

Figure 8: Time-history of horizontal velocity at 8 positions in front of the wall, 25mm above flat bed, f=0.9Hz, H=50mm. The node is at x=-0.31m (posn.4) approximately; x=-0.062m (posn.1) and x=-0.558m (posn.7) correspond approximately to the shoreward and seaward limits of movement; x=-0.62m (posn.8) corresponds to the offshore antinode. The solid line is the velocity predicted using Stokes 2nd order theory; the discrete symbols are the LDA measurements of the velocity.

A vortex grows in the lee of a ripple as the main flow velocity decreases from maximum velocity to zero velocity at flow reversal. Vortex growth on the antinodal side of a ripple occurs as the main flow acceleration is increasing from zero to maximum acceleration towards the node and vortex growth on the nodal side of a ripple occurs as the main flow acceleration is increasing from zero to maximum acceleration towards the antinode. Because the maximum acceleration towards the node is greater than the maximum acceleration towards the antinode, a larger vortex forms on the antinodal side of the ripple than on the nodal side. The larger vortex entrains more sand as it grows making it available for transport towards the node as the flow reverses.

Figure 9 presents PIV-measured vector plots of the flow over and around a ripple located at a position between 2 and 3 in Figure 8. Flow to the left is towards the wall/antinode; flow to the right is towards the node. Six vector plots are shown corresponding to 6 different phases of the wave. In Figure 9(a) the main flow has just started to decrease from maximum velocity towards the wall. The beginning of the vortex growth on the antinodal side of the ripple can be seen. Figure 9(b) shows the vortex well established as the flow reversal stage is approached while Figure 9(c) shows flow reversal with the vortex lifting off the bed. Figure 9(d) shows the situation before maximum velocity towards the node is reached while 9(e) and 9(f) show the vortex growth on the nodal side of the ripple with 9(f) corresponding to flow reversal.

Figure 9 clearly illustrates the asymmetry in vortex generation: a much larger vortex is formed on the antinodal side of the ripple than on the nodal side. As a result, when the bed is mobile, a larger volume of sand is entrained by the larger vortex on the antinodal side of the ripple than is entrained by the smaller vortex on the nodal side half a wave cycle later. The larger volume of sand is available for transport towards the node at flow reversal, while the smaller volume is available for transport towards the antinode. Therefore, the effect over a complete wave cycle is net transport of material towards the node.

The present description of the role played by the vortices in determining the net sand transport under standing waves echoes what has been observed by others for the case of nonlinear progressive waves (e.g. Sato and Horikawa (1986). Like the standing wave case, vortex growth is not the same on the two sides of a ripple in the case of non-linear progressive waves. However the reason for the asymmetry in vortex growth is not the same for progressive and standing waves: in the case of non-linear progressive waves the velocity function is skewed with the maximum shoreward velocity greater than the maximum seaward velocity. The result is larger vortex growth on the shoreward side of the ripple as the flow velocity decreases from maximum velocity shoreward to zero velocity at flow reversal. The net effect is greater sand transport seaward than shoreward.

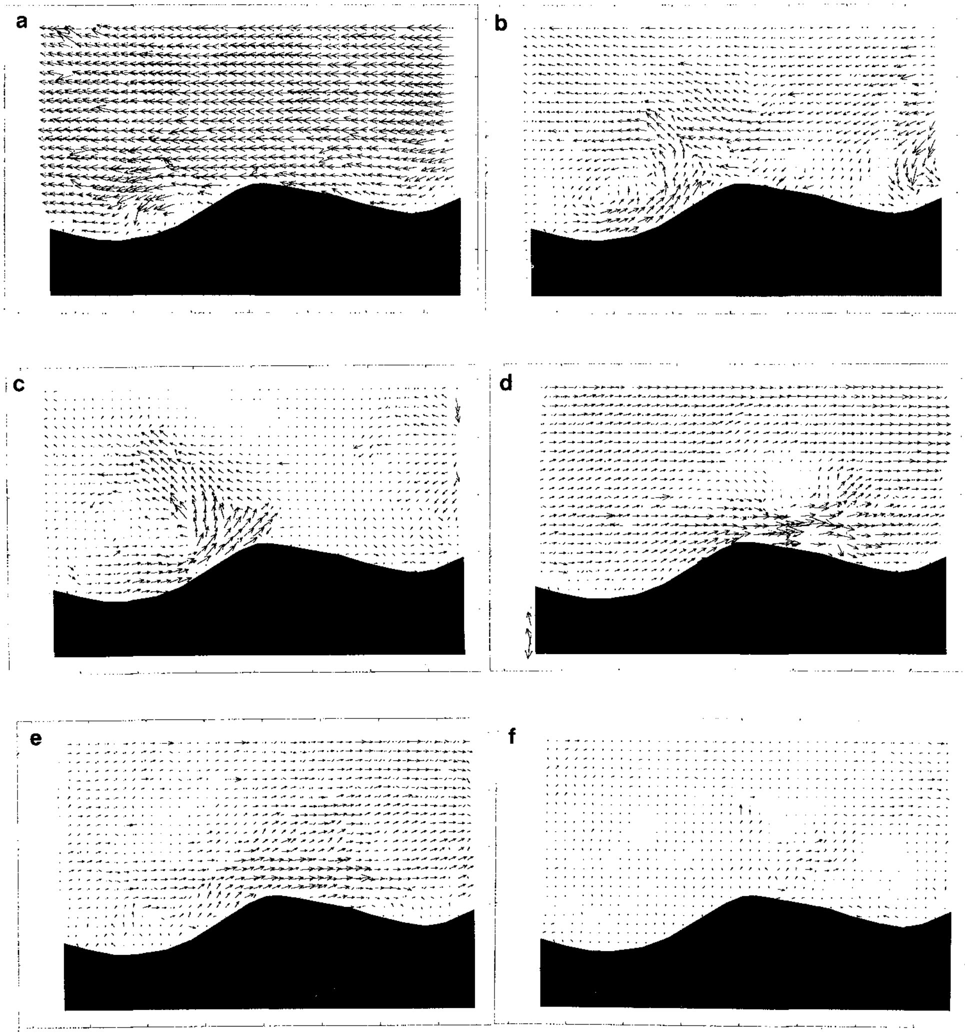

Figure 9: PIV-measured velocity fields corresponding to 6 phases of the wave, f=0.9Hz, H=50mm; the ripple shown is located between positions 2 and 3 in Figure 8.

Conclusions

Two main aspects of N-type beach response in front of wave-reflecting structures have been studied: (i) the characteristics of the equilibrium beach profile and (ii) the underlying mechanism causing sand transport towards the node.

The major features of the underlying larger bedforms of the equilibrium beach profile are well characterised by an equation which is fully defined for a given wave condition if the positions of the limits of movement and the amplitude factor a are known. The limits of movement can be estimated using an incipient motion condition although good agreement was not achieved in the present study between the predicted and measured shoreward limits. For the sand used in the study the amplitude factor a is approximately 1/25th of the equilibrium bed profile wavelength λ_b; maximum scour depth is therefore approximately 1/30th of λ_b. Further work is needed at larger scale with different sand sizes to see if these results have general application.

The ripples superimposed on the larger bedforms play a crucial role in the sand transport process. Asymmetry in the main flow velocity time-history, resulting from the superposition of non-linear incident and reflected waves, causes larger vortex growth on the antinodal side of the ripple than on the nodal side. Because vortex growth occurs as the flow is slowing down and the vortex is at its largest and lifting off the bed at flow reversal, more sand is transported towards the node than towards the antinode with each wave cycle. PIV is a very effective way of studying the flow over and around the ripples.

Acknowledgements

Mr. Seaman acknowledges the support of Aberdeen University through the receipt of an Aberdeen University Research Studentship. The assistance of Bill Lowson with the laboratory work is gratefully acknowledged.

References

de Best, A., Bijker, E.W., and Wichers, J.E.W., (1971), *Scouring of a Bed in Front of a Vertical Breakwater,* Proc. 1st P.O.A.C. Conf., Vol. II, p1077-1086.

Carter, T.G., Liu, P.L-F., and Mei, C.C. (1973), *Mass transport by waves and Offshore sand bedforms*, ASCE, Journ. Waterways, Harbours and Coastal Engineering, Vol 99, no. ww2, p165-184.

Irie, I., and Nadaoka, K., (1984), *Laboratory Reproduction of Seabed Scouring Front of Breakwaters,* Proc. 19th Conf. on Coastal Engineering, p1715-1731.

Longuet-Higgins, M.S. (1953), *Mass Transport in Water Waves*, Phil. Trans. Royal Society of London, Vol 245, p535-581

Losada, M.A., and Desire, J.M., (1985), *Incipient Motion on a Horizontal Granular Bed in Non-breaking Water Waves,* Coastal Engineering, 9, p357-369.

Sato, S. and Horikawa, K. (1986), *Laboratory Study on Sand Transport over Ripples due to Asymmetric Oscillatory Flows*, Proc. 20th Coastal Engng. Conf., Chap. 109, p1481-1489

Xie, S., (1985), *Scouring Patterns in Front of Vertical Breakwaters,* Acta Oceanologica Sinica, Vol. 4, No. 1, p153-164.